

**Transition of a two-dimensional spin mode to a helical state by lateral confinement**P. Altmann,<sup>1</sup> M. Kohda,<sup>1,2</sup> C. Reichl,<sup>3</sup> W. Wegscheider,<sup>3</sup> and G. Salis<sup>1,\*</sup><sup>1</sup>*IBM Research–Zurich, Säumerstrasse 4, 8803 Rüschlikon, Switzerland*<sup>2</sup>*Department of Materials Science, Tohoku University, 980-8579 Sendai, Japan*<sup>3</sup>*Solid State Physics Laboratory, ETH Zurich, 8093 Zurich, Switzerland*

(Received 2 October 2015; revised manuscript received 15 November 2015; published 14 December 2015)

Spin-orbit interaction enables electrical tuning of spins, thus facilitating spintronics applications. It leads to spin precession about a momentum-dependent spin-orbit field. For a diffusive, two-dimensional electron gas the spin orientation at a given spatial position depends on which trajectory the electron travels to that point. Under increasing lateral confinement the spin orientation becomes independent on the trajectory and the formation of a long-lived helical spin mode is predicted. Here we visualize this transition experimentally in a GaAs quantum-well structure with isotropic spin-orbit interaction. Spatially resolved measurements show the formation of a helical mode already for nonquantized and nonballistic channels. We find a spin-lifetime enhancement that is in excellent agreement with theoretical predictions. Lateral confinement of a two-dimensional electron gas provides an easy-to-implement technique for achieving long spin lifetimes in the presence of strong spin-orbit interaction for a wide range of material systems.

DOI: [10.1103/PhysRevB.92.235304](https://doi.org/10.1103/PhysRevB.92.235304)

PACS number(s): 72.25.Dc, 71.70.Ej, 72.25.Rb

**I. INTRODUCTION**

Electron spins in semiconductor quantum structures are very promising for future spintronic applications. Spin-orbit interaction (SOI) in these systems provides a convenient way for electrical tuning of spins [1–3]. It can be described by an effective magnetic field about which the electron spins precess. In a diffusive electron system with intrinsic SOI (e.g., of Rashba or Dresselhaus type), the effective spin-orbit field changes after each scattering event. This leads to a randomization of spin polarization that is, in the case of an initially homogenous spin excitation, known as the Dyakonov-Perel (DP) spin-dephasing mechanism [4]. A local spin excitation evolves into a spin mode that is described by the Green's function of the spin diffusion equation [5–7]. For a two-dimensional (2D) system in the weak SOI limit, this mode can be calculated analytically for a few special situations, such as for the persistent spin helix case with equal Rashba and Dresselhaus SOI [8–12]. In the isotropic limit (either only Rashba or only linear Dresselhaus SOI), it is described by a Bessel-type oscillation in space [see Fig. 1(b)] [5]. Its spin lifetime is only slightly enhanced [5] compared with the DP time because rotations about varying precession axes [see Figs. 1(c)–1(e)] do not commute and therefore the spin polarization at a given position depends on the trajectory by which the electron reaches that position. If the electron motion is laterally confined by a sufficiently small channel structure of width  $w$ , the spin motion is restricted to a ring on the Bloch sphere [see Figs. 1(g) and 1(h)]. In this situation, the spins collectively precess as they move along the channel direction [Fig. 1(f)] [13–15]. This regime is entered when the cumulative spin rotations attributed to the transverse motion are small, i.e., if  $wq^0 < 1$ , where  $q^0$  is the wave number of the 2D spin mode. The spin-orbit length is related to  $q^0$  via  $\lambda_{SO} = 2\pi/q^0$ . As a consequence, for a 2D diffusive system, increasing lateral confinement is predicted [13,14] to result in a suppressed spin decay proportional to  $(q^0 w)^2$ . This effect could be highly

relevant for spintronics applications because it circumvents the conventional trade-off between a long spin lifetime and strong SOI. It has been experimentally explored in different ways, including measurements of weak antilocalization [16,17], the inverse spin-Hall effect [18], and time-resolved Kerr rotation [19]. However, none of these works were able to resolve the spin dynamics both spatially and temporally, and, thus, a quantitative investigation of the spin mode in the confined channel is still lacking.

Here, we experimentally explore the dynamics and spatial evolution of electron spins in a 2D electron gas hosted in a symmetrically confined, 12-nm-wide GaAs/AlGaAs quantum well where the linear Dresselhaus SOI is much larger than the Rashba or the cubic Dresselhaus SOI, thus providing an almost isotropic SOI. We study the transition from such a 2D system to a one-dimensional (1D) channel by lithographically defining wire structures along the  $[1\bar{1}0]$  ( $x$ ) and  $[110]$  ( $y$ ) directions with a lateral width  $w$  ranging from 700 nm to 79  $\mu\text{m}$ . Time-resolved Kerr rotation measurements with high spatial resolution reveal the transition from a radially symmetric mode in the 2D case to a helical mode where spin polarization is rotated along the channel direction in the 1D case. The spin lifetime of the observed modes are in excellent agreement with theoretical predictions. We find that, in the diffusive 1D case, the lifetime is limited by cubic Dresselhaus SOI to the same value as in the 2D spin helix case.

**II. EXPERIMENT**

Figure 1(a) shows a sketch explaining the measurement principle. Spins polarized along the out-of-plane direction,  $z$ , are locally excited at time  $t = 0$  by a focused, circularly polarized pump laser pulse, which has a Gaussian intensity profile with a sigma width of 1.1  $\mu\text{m}$ . A second, linearly polarized probe pulse measures the out-of-plane component,  $S_z$ , of the local spin density using the magneto-optical Kerr effect. The focused probe beam (time-averaged power 50  $\mu\text{W}$ ) is located at a position  $(x, y)$  relative to the pump spot (time-averaged power 100  $\mu\text{W}$ ) [Fig. 1(a)]. Two Ti:sapphire lasers are used

\*gsa@zurich.ibm.com

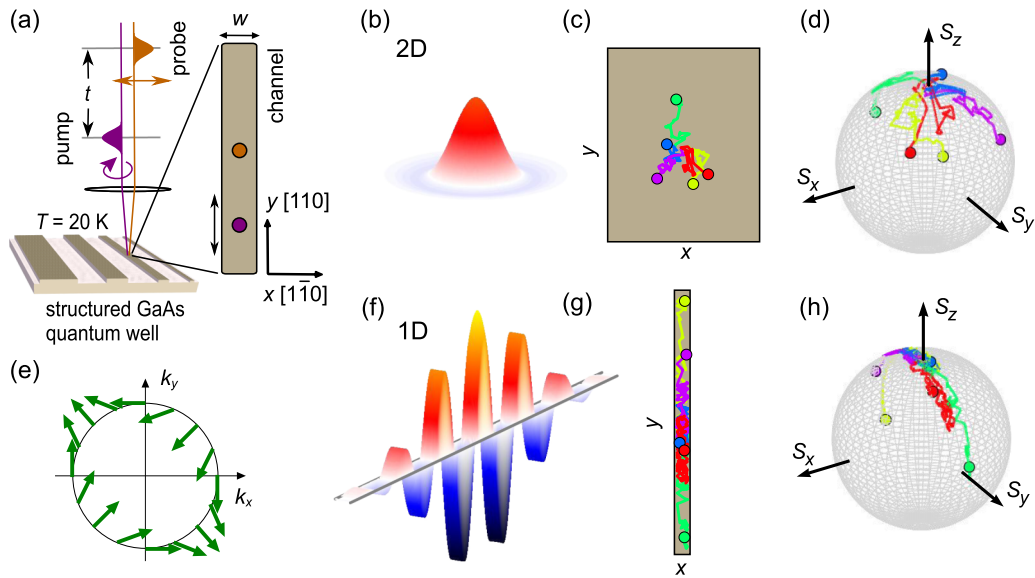


FIG. 1. (Color online) Measurement principle and expected spin modes. (a) A focused pump laser pulse locally excites out-of-plane spin polarization  $S_z$  with a Gaussian width of  $\approx 1.1 \mu\text{m}$ . A probe laser pulse measures the local spin distribution after a time delay  $t$  via the magneto-optical Kerr effect. Pump and probe spots are spatially scanned against each other. (b) In the 2D case, spin diffusion in the isotropic SOI field, (e), evolves a local spin excitation along  $z$  into a Bessel-type spin mode, whose  $S_z$  component is shown (red color indicates positive, blue color negative  $S_z$ ). The spin trajectories in the 2D plane, (c), are partially correlated with the trajectories on the Bloch sphere, (d), such that the local spin density decays more slowly than that of the whole ensemble. (f) In the 1D case, the emerging spin mode is long-lived and described by a cosine oscillation of  $S_z$ , corresponding to a helical rotation of the spin polarization. (g) The lateral confinement restricts the diffusive trajectories in real space, such that the spins on the Bloch sphere evolve on a ring, (h), whose width scales with the channel width,  $w$ . The smaller  $w$  is, the more the spins precess about a single axis, leading to a drastic increase of the lifetime of the helical mode.

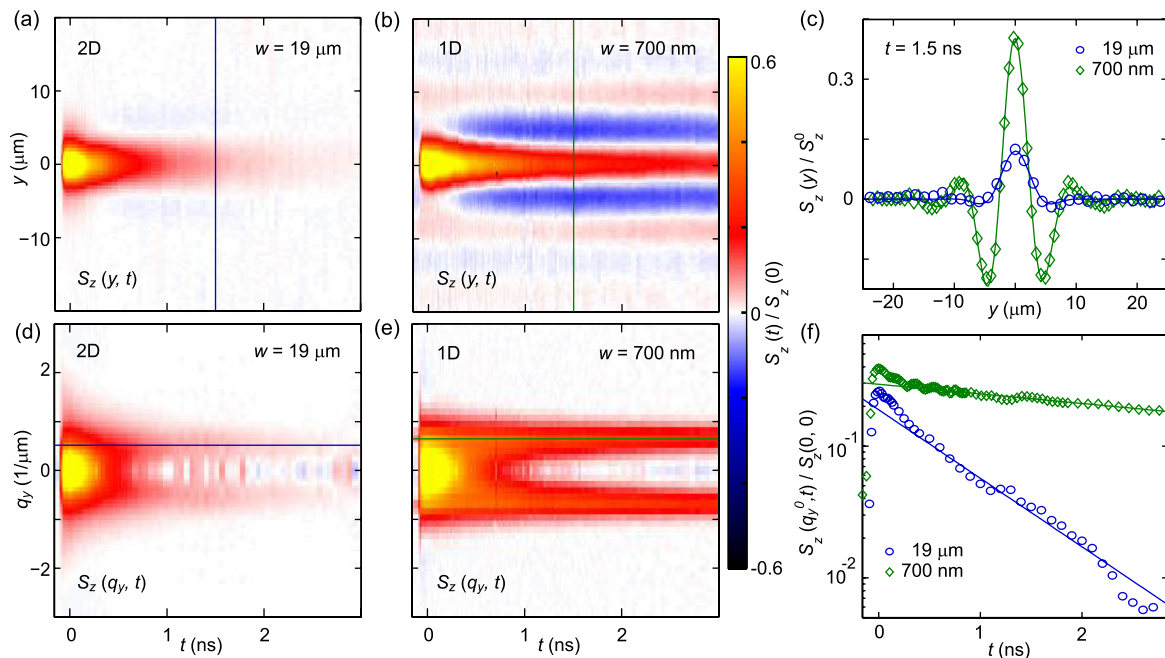


FIG. 2. (Color online) Direct mapping of spin precession and spin decay. (a),(b) Spatial maps along the channel direction  $y$  of the out-of-plane spin density  $S_z$  for varying time delays  $t$  between the pump and probe laser pulses. The  $19\text{-}\mu\text{m}$ -wide channel, (a), represents a 2D situation, whereas the  $700\text{-nm}$ -wide channel, (b), is close to the 1D limit and exhibits a long-lived mode with oscillating  $S_z(y)$  [sign encoded as red (+) and blue (-)]. The mode from the preceding laser pulse (pulse period  $12.6\text{ ns}$ ) is still visible at negative delay. (c) Line cuts through the data of (a) and (b) at  $t = 1.5\text{ ns}$  for comparison (symbols). Solid lines are fits to the data. (d) and (e) show the Fourier transform of  $S_z(y)$  for the  $19\text{-}\mu\text{m}$  and  $700\text{-nm}$  channels, respectively. For  $w = 700\text{ nm}$ , the initially Gaussian spectrum quickly converges to a long-lived spin mode at finite  $q_y = q_y^0$  (position indicated as blue and green horizontal lines). (f) Line cuts through the data of (d) and (e) at  $q_y \approx q_y^0$ . At each  $q_y$ , the amplitude decays biexponentially, with the longer-lived mode visible at longer  $t$ .

to generate the pump and probe laser pulses at 785 nm and 802 nm, respectively. Pulse lengths are on the order of 1 ps and the repetition rate is 79.1 MHz, which corresponds to 12.6 ns between two pulses. The spatial evolution of the spin packet is mapped out along the channel direction for various time delays,  $t$ , between pump and probe pulses. All measurements have been performed at a sample temperature of 20 K.

A GaAs quantum well is grown on a (001) GaAs substrate by molecular beam epitaxy. The barrier material is  $\text{Al}_{0.3}\text{Ga}_{0.7}\text{As}$ . Front and back Si  $\delta$ -doping layers are positioned such that the electric field perpendicular to the quantum-well plane is small. A sheet density of  $n_s = 3.5 \times 10^{15} \text{ m}^{-2}$  and a transport mobility of  $7.0 \times 10^5 \text{ cm}^2(\text{Vs})^{-1}$  were determined at 4 K after illumination by a van der Pauw measurement. Wires of variable width were processed with photolithography and wet-chemical etching. The effective widths,  $w$ , of the wires were determined by scanning electron microscopy images, measuring the width of the top surface.

A measurement of spatially resolved spin dynamics in a channel in the 2D limit ( $w = 19 \mu\text{m}$ ) is shown in Fig. 2(a). Spins are excited at  $t = 0$  and at  $x = y = 0$  and traced as a function of  $y$  and  $t$ . At  $y = 0$ ,  $S_z$  simply decays in time. It reverses its sign after  $t > 400$  ps for electrons that diffused along  $y$  by more than  $\approx 4 \mu\text{m}$ , seen as a faint blue color in the figure. The situation is different in the 700-nm-wide channel [Fig. 2(b)]. Here, spin decay is strongly suppressed and  $S_z$  reverses its sign multiple times along  $y$ . Note that the pattern is overlaid with the spin texture that survived from the previous pump pulse at  $t = -12.6$  ns. Figure 2(c) shows measured data of  $S_z(y)$  for the 19- $\mu\text{m}$  and the 700-nm-wide channels taken at  $t = 1.5$  ns (symbols). The lines are fits to a zeroth order Bessel function (700 nm) and to the product of a cosine and a Gaussian function (19  $\mu\text{m}$ ). The comparison of the two curves clearly shows an enhanced  $S_z$  and strong oscillations along  $y$  in the narrow channel. This indicates a helical spin mode in the 1D case. The helical nature is further supported by measured maps where an external magnetic field is applied along the  $x$  direction, rotating the helix as a function of time; see Appendix A.

### III. EVALUATION

For a deeper analysis, it is advantageous to Fourier transform  $S_z(x, y, t)$  to obtain Fourier components  $S_z(q_x, q_y, t)$  at wave numbers  $q_x$  and  $q_y$  that, according to theory, decay biexponentially in time [6]. For channels narrower than 15  $\mu\text{m}$ , the spin modes exhibit a pronounced structure only along the channel direction, and it is therefore sufficient to analyze the 1D Fourier transformation along this direction. For a channel along the  $y$  direction, the Fourier transformation is given by

$$S_z^{\text{1D}}(q_y, t) = \int_{-\infty}^{\infty} \cos(q_y y) S_z(y, t) dy. \quad (1)$$

For wider channels, we obtain the 2D Fourier transformation from 1D scans of  $S_z$  by assuming a radially symmetric spin mode. This is justified because we observe a similar dependence of  $S_z$  along the  $x$  and  $y$  directions, as seen from the values obtained for wavenumbers  $q_x^0$  and  $q_y^0$  later in the text. The Fourier transform is then given by

$$S_z^{\text{2D}}(q_y, t) = \int_{-\infty}^{\infty} \pi |y| J_0(q_y y) S_z(y, t) dy. \quad (2)$$

Here,  $J_0$  is the zeroth-order Bessel function. Figures 2(d) and 2(e) show  $S_z^{\text{2D}}(q_y, t)$  for the 19- $\mu\text{m}$  wire and  $S_z^{\text{1D}}(q_y, t)$  for the 700-nm wire, respectively. The rate with which the initially Gaussian distribution of  $S_z(q_y, t)$  decays in time varies with  $q_y$  and is minimal at a finite wave number  $q_y^0$ . Figure 2(f) shows traces at  $q_y \approx q_y^0$  for both wires. For  $t > 500$  ps, we fit each trace with a single exponential decay to obtain the momentum-dependent lifetime  $\tau(q_y)$  of the longer-lived spin mode [6,10]. The decay rates,  $1/\tau(q_y)$  are shown in Fig. 3(a). In both the 1D and the 2D case,  $1/\tau$  vs  $q_y$  can be well approximated close to  $q_y^0$  by the parabolic function [6,7]

$$1/\tau = 1/\tau^0 + D_s (q_y - q_y^0)^2, \quad (3)$$

where  $D_s = 50 \text{ cm}^2/\text{s}$  is the spin diffusion constant. Note that the spin diffusion constant differs from the electron diffusion

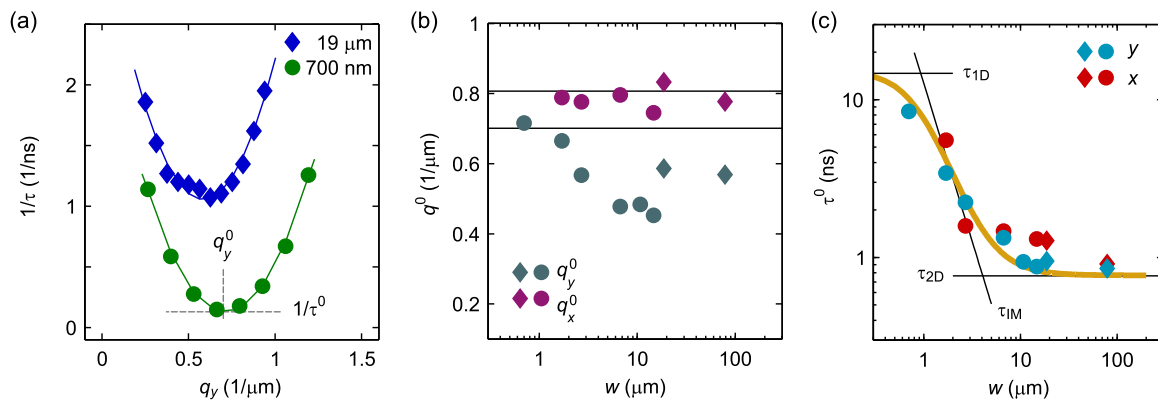


FIG. 3. (Color online) Fit results. (a) Decay rates for the 19- $\mu\text{m}$ -wide (diamonds) and 700-nm-wide (dots) channels along the  $y$  direction as a function of the wave number,  $q_y$ . Data is obtained from fitting to  $S_z(q_y, t)$  an exponential decay for  $t > 500$  ps, thus corresponding to the long-lived mode. Solid lines are parabolic fits of the decay rate versus  $q$ , from which the position,  $q_y^0$ , and the lifetime,  $\tau^0$ , of the evolving spin mode are obtained. (b) Values for the spin-mode wave numbers  $q_x^0$  and  $q_y^0$ , shown for measurements at various channel widths,  $w$ , along the  $x$  and  $y$  direction. (c) Lifetime of spin modes,  $\tau^0$ , as a function of  $w$  and for both channel directions. Solid black lines are the theoretically expected lifetimes. The yellow solid line is their interpolation. In all three plots, circles (diamonds) stand for fit values obtained from 1D (2D) Fourier transformations.

constant determined from transport measurements because it is sensitive to electron-electron scattering [20,21]. Figures 3(b) and 3(c) plot the values obtained for  $q^0$  and  $\tau^0$ , respectively, for channels along the  $y$  and  $x$  directions and of various widths. Values of  $\tau^0$  obtained with 2D and 1D Fourier transformations for all  $w$  are shown in Appendix B.

Comparing  $q_x^0$  and  $q_y^0$  in Fig. 3(b), we observe a slight anisotropy characterized by  $q_x^0 > q_y^0$ . This means that the SOI is stronger for electrons that move along  $x$  and indicates a remaining Rashba field due to a slight asymmetry in the quantum well. The SOI coefficients,  $\alpha$  and  $\beta$ , are obtained from  $q_y^0$  and  $q_x^0$  measured in the 1D limit [solid lines in Fig. 3(b)] by using the expressions

$$q_y^0 = \left| \frac{2m^*}{\hbar^2}(\alpha + \beta) \right| \approx 0.7 \mu\text{m}^{-1}, \quad (4)$$

and

$$q_x^0 = \left| \frac{2m^*}{\hbar^2}(\alpha - \beta) \right| \approx 0.8 \mu\text{m}^{-1}. \quad (5)$$

Here,  $m^*$  is the effective electron mass,  $\hbar$  is the reduced Planck's constant,  $\alpha$  is the SOI parameter of the Rashba field, and  $\beta = \beta_1 - \beta_3$  is that of the Dresselhaus field.  $\beta_1$  and  $\beta_3$  characterize the linear and cubic Dresselhaus fields, respectively. We find  $\alpha = -0.3 \times 10^{-13}$  eVm and  $\beta_1 = 4.9 \times 10^{-13}$  eVm. Here, we assumed  $\beta_3 = -\gamma\pi n_s/2 = 0.6 \times 10^{-13}$  eVm, given the Dresselhaus parameter  $\gamma = -11 \times 10^{-30}$  eVm<sup>3</sup> [22].

The dependence of  $q_x^0$  on  $w$  is rather flat, whereas  $q_y^0$  decreases for increasing  $w$ . This is in agreement with the prediction that  $q_y^0$  of the 2D spin mode is smaller for slightly anisotropic SOI than expected from Eq. (5) [6,23]. Close to the persistent spin helix situation, the same effect leads to a suppression of precession along  $y$ .

The lifetime,  $\tau^0$ , however, behaves almost identically for both wire directions and increases by about one order of magnitude from  $w = 19 \mu\text{m}$  to 700 nm. Theory provides expressions for the lifetime in the 2D limit,  $\tau_{2D}$ , (Dresselhaus SOI only) [5,6] and in the intermediate regime [13,14],  $\tau_{IM}$ :

$$\tau_{2D}^{-1} = 8 \frac{D_s m^{*2}}{\hbar^4} \left[ \frac{7}{32} \beta^2 + \frac{11}{16} \beta_3^2 \right], \quad (6)$$

$$\tau_{IM} = 48 \tau_{DP} (q^0 w)^{-2}. \quad (7)$$

Here,  $\tau_{DP}$  is the Dyakonov-Perel spin dephasing time, which is given by

$$\tau_{DP}^{-1} = 8 \frac{D_s m^{*2}}{\hbar^4} (\alpha^2 + \beta^2 + \beta_3^2). \quad (8)$$

For very narrow channels, the lifetime  $\tau_{1D}$  is limited by cubic Dresselhaus SOI only, and as we will show later, is the same as in the completely balanced spin-helix case [24]:

$$\tau_{1D}^{-1} = 6 \frac{D_s m^{*2}}{\hbar^4} \beta_3^2. \quad (9)$$

The theoretically expected values are plotted in Fig. 3(c) as black lines. The interpolation between  $\tau_{2D}$ ,  $\tau_{IM}$ , and  $\tau_{1D}$  [yellow line in Fig. 3(c)] is in very good quantitative agreement with the experimental data. Although  $\tau^0$  towards smaller  $w$  is not yet saturated, it is possible to project that cubic SOI will limit the lifetime.

#### IV. MONTE CARLO SIMULATIONS

Spin dynamics in a laterally confined 2D electron gas are calculated numerically using a Monte Carlo method where the positions and spin orientations of  $3 \times 10^5$  electrons are updated in time steps of 0.1 ps. Electrons are distributed on a Fermi circle and scatter isotropically, with the mean scattering time given by  $\tau = 2D_s/v_F^2$ , where  $v_F = \hbar k_F/m$  is the Fermi velocity. Each electron moves with the Fermi velocity and sees an individual spin-orbit field as defined in the supplementary information of Ref. [12] that depends on its velocity direction. The real-space coordinates and the corresponding spin dynamics are calculated semiclassically. We initialize the electrons at  $t = 0$ , all with their spins oriented along the  $z$  direction, and distribute their coordinates in a Gaussian probability distribution with a center at  $x = y = 0$  and a sigma width of 500 nm. Histograms of the electron density and the spin orientations are recorded every 5 ps, and the simulation is run until  $t = 5$  ns is reached. We obtain the spin polarization at  $x = y = 0$  versus  $t$  from the spin-density maps using a convolution with an assumed Gaussian probe spot size of 500 nm. We determine the spin lifetimes  $\tau^0$  by fitting the transients with a function proportional to  $1/t \times \exp -t/\tau^0$  or  $1/\sqrt{t} \times \exp -t/\tau^0$  in a window  $800 \text{ ps} < t < 4000 \text{ ps}$ , where additional spin decay is negligible because of the small spot sizes [24]. For the data shown in Fig. 4, we have used the following parameters:  $D_s = 40 \text{ cm}^2/\text{s}$ ,  $n_s = 3.4 \times 10^{15} \text{ cm}^{-2}$ ,  $\beta_1 = 4.9 \times 10^{-13} \text{ eVm}$ , and  $\beta_3 = 0.6 \times 10^{-13} \text{ eVm}$ . Lateral confinement was implemented by assuming specular scattering at the channel edges. For the 1D case,  $w = 400 \text{ nm}$  was used.

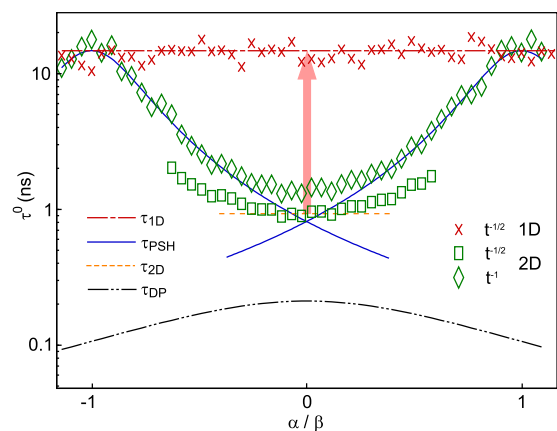


FIG. 4. (Color online) Lifetime enhancement for various  $\alpha/\beta$ . Spin lifetimes for the 1D and 2D situation as determined from Monte Carlo simulations for various ratios of  $-1.1 < \alpha/\beta < 1.1$ . Data is obtained by fitting  $S_z(y, t)$  with a model that includes a diffusive dilution proportional to either  $1/t$  or  $1/\sqrt{t}$ . The former is used in the 2D case for  $|\alpha| \approx |\beta|$  (diamonds), the latter for isotropic SOI in the 2D case (rectangles) and for the 1D case (crosses). The red, blue, orange, and black lines are theoretical curves for  $\tau_{1D}$ ,  $\tau_{PSH}$ ,  $\tau_{2D}$ , and  $\tau_{DP}$ , respectively. The lifetime enhancement under lateral confinement is largest for  $\alpha = 0$  (arrow). For both the 2D case at  $|\alpha| = |\beta|$  and the 1D case, the lifetime is limited by the same value given by the cubic SOI only.

The lifetime enhancement achievable by channel confinement depends strongly on the ratio  $\alpha/\beta$ . Figure 4 shows lifetimes determined by Monte Carlo simulations for  $-1.1 < \alpha/\beta < 1.1$ . Without Fourier transformation one has to account for a diffusive factor that reduces the amplitude, in addition to an exponential decay term. The diffusive dilution of electrons in 2D scales with  $1/t$  and in 1D with  $1/\sqrt{t}$ . Interestingly, the spins in a 2D system, however, also decay with  $1/\sqrt{t}$  for the isotropic SOI case [6,25]. The lines are the theoretically expected values of  $\tau^0$  for 2D and 1D spin modes ( $\tau_{1D}$ ,  $\tau_{2D}$ ), as well as for the DP case ( $\tau_{DP}$ ). For a situation close to  $\alpha \approx \beta$ , the spin lifetime,  $\tau_{PSH}$ , can be given analytically [24]:

$$\tau_{PSH}^{-1} = 2D_s \frac{m^*2}{\hbar^4} [(\alpha - \beta)^2 + 3\beta_3^2]. \quad (10)$$

It is plotted as a solid blue line in Fig. 4. This formula provides a good approximation of the spin lifetime also further away from  $\alpha \approx \beta$ . We find that in a narrow channel (red crosses in Fig. 4),  $\tau^0$  does not depend on  $\alpha$  or  $\beta_1$  and is limited by cubic SOI ( $\beta_3$ ) only. The same limit is reached in the 2D situation (green symbols in Fig. 4) at  $|\alpha| = |\beta|$ , i.e., when the system is tuned to the persistent spin helix symmetry. The maximal lifetime enhancement under lateral confinement in the diffusive limit occurs for the isotropic case ( $\alpha = 0$ ). Close to  $|\alpha| = |\beta|$ , the lifetime enhancement is small, but a reduction of diffusive dilution was observed [26].

## V. CONCLUSION AND OUTLOOK

In conclusion, we measured the evolution of a local spin excitation in a GaAs/AlGaAs quantum well dominated by linear Dresselhaus SOI. The lateral confinement leads to an increased correlation between electron position and spin precession angle. Using a real-space mapping of the time-resolved spin distribution, we observe a transition to a helical spin mode accompanied by an enhanced lifetime for decreasing channel width. The transition occurs for a channel width close to the spin-orbit length. The analysis in Fourier space shows that the long-lived components decay exponentially with a minimum rate at a finite  $q^0$ . Both the precession length and the lifetime are in quantitative agreement with theory for the 2D limit, the 1D limit, and also for the intermediate regime. The narrowest channel in our study still is 10 times wider than the mean free path (including electron-electron scattering) and 100 times wider than the Fermi wavelength of the electrons. At those smaller length scales, also a reduction of the cubic SOI contribution to spin decay is expected [27].

These findings illuminate an interesting path for studying spin-related phenomena. Lateral confinement in the nm range provides a straightforward method for achieving spin lifetimes that are otherwise only possible by careful tuning of SOI to the persistent spin helix symmetry. This facilitates the use of spins in group-IV semiconductors, like Si and Ge, but also in materials with stronger SOI, such as InAs or GaSb where the spin-orbit length is expected to be on the order of a few nm. Extending the presented method to 1D systems in the quantized limit will be relevant for the quest for Majorana fermions [28–31]. Furthermore, the results are important for

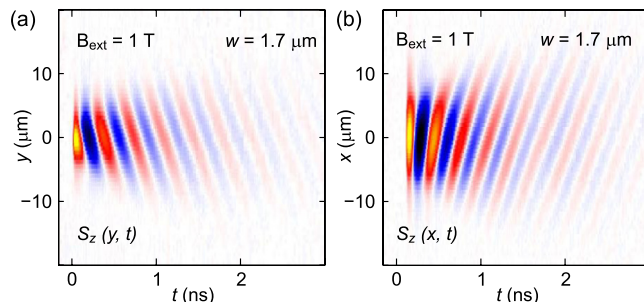


FIG. 5. (Color online) Spin maps at an external magnetic field. (a)  $S_z(y, t)$  in a  $1.7\text{-}\mu\text{m}$ -wide wire along the  $y$  direction at an external magnetic field of  $B_{\text{ext}} = 1$  T along the  $-x$  direction. The sample temperature is 30 K. (b)  $S_z(x, t)$  in a  $1.7\text{-}\mu\text{m}$ -wide wire along the  $x$  direction at an external magnetic field of  $B_{\text{ext}} = 1$  T along the  $+y$  direction. The sample temperature is 10 K. The magnetic field induces additional spin precession in time. The tilted lines of constant phase show the helical nature of the spin mode. From the similar strength but opposite signs of the tilts in the  $(x, t)$  and the  $(y, t)$  planes, it is concluded that  $|\beta| > |\alpha|$ . Moreover, the tilt in (b) is slightly stronger than in (a), which means that  $\alpha$  is negative.

transport studies and spintronics applications [8,32,33] using SOI in 1D or quasi-1D systems.

## ACKNOWLEDGMENTS

We acknowledge financial support from the Swiss National Science Foundation through NCCR QSIT and from the Ministry of Education, Culture, Sports, Science, and Technology (MEXT) via Grants-in-Aid for Scientific Research No. 15H02099 and No. 25220604. We thank R. Allenspach, A. Fuhrer, T. Henn, A. V. Poshakinskiy, F. Valmorra, M. Walser, and R. J. Warburton for helpful discussions, and U. Drechsler for technical assistance.

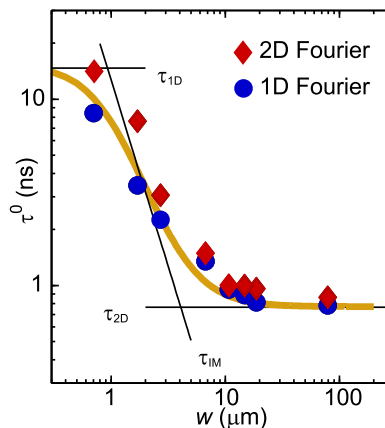


FIG. 6. (Color online) Comparison of radial and linear Fourier transformations. Experimental values of  $\tau^0$  as obtained by 2D (diamonds) and 1D (circles) Fourier transformations of  $S_z(y, t)$ . Also shown are the theoretical values of  $\tau_{1D}$ ,  $\tau_{2D}$ , and  $\tau_{IM}$ , as well as their interpolation.

**APPENDIX A: EXTERNAL MAGNETIC FIELD**

An applied external magnetic field superposes with the spin-orbit field. If the field is applied along the direction of the spin-orbit field that generates a helical spin mode, the helix is rotated as a function of time, which can be seen as tilted lines of constant spin precession phase in measured spatial spin maps. Figure 5 shows such maps measured on wires along the  $x$  and  $y$  directions with an external magnetic field of 1 T applied along the  $y$  and  $-x$  directions, respectively. The opposite tilt of the lines of constant phase indicates the dominance of Dresselhaus SOI over Rashba SOI. Because  $\alpha < 0$ , we observe a slightly

steeper slope  $dy/dt$  for the wire along  $x$  [Fig. 5(a)] compared to  $-dx/dt$  for the wire along  $y$  [Fig. 5(b)].

**APPENDIX B: FOURIER TRANSFORMATION**

We have Fourier transformed the data sets for different  $w$  with both, 1D and 2D Fourier transformations according to Eqs. (1) and (2). Figure 6 shows  $\tau^0$  along the  $y$  direction determined from both transformations. In Fig. 3, we plot the 2D transformation for  $w \geq 15 \mu\text{m}$  and the 1D transformation for narrower channels.

- 
- [1] Y. Kato, R. C. Myers, A. C. Gossard, and D. D. Awschalom, *Nature (London)* **427**, 50 (2004).
- [2] K. C. Nowack, F. H. L. Koppens, Y. V. Nazarov, and L. M. K. Vandersypen, *Science* **318**, 1430 (2007).
- [3] L. Meier, G. Salis, I. Shorubalko, E. Gini, S. Schoen, and K. Ensslin, *Nat. Phys.* **3**, 650 (2007).
- [4] M. I. Dyakonov and V. I. Perel', *Sov. Phys. Solid State* **13**, 3023 (1972).
- [5] V. A. Frolov, *Phys. Rev. B* **64**, 045311 (2001).
- [6] T. D. Stanescu and V. Galitski, *Phys. Rev. B* **75**, 125307 (2007).
- [7] X. Liu and J. Sinova, *Phys. Rev. B* **86**, 174301 (2012).
- [8] J. Schliemann, J. C. Egues, and D. Loss, *Phys. Rev. Lett.* **90**, 146801 (2003).
- [9] B. A. Bernevig, J. Orenstein, and S.-C. Zhang, *Phys. Rev. Lett.* **97**, 236601 (2006).
- [10] J. D. Koralek, C. P. Weber, J. Orenstein, B. A. Bernevig, Shou-Cheng Zhang, S. Mack, and D. D. Awschalom, *Nature (London)* **458**, 610 (2009).
- [11] M. Kohda, V. Lechner, Y. Kunihashi, T. Dollinger, P. Olbrich, C. Schönhuber, I. Caspers, V. V. Bel'kov, L. E. Golub, D. Weiss, K. Richter, J. Nitta, and S. D. Ganichev, *Phys. Rev. B* **86**, 081306(R) (2012).
- [12] M. P. Walser, C. Reichl, W. Wegscheider, and G. Salis, *Nat. Phys.* **8**, 757 (2012).
- [13] A. G. Mal'shukov and K. A. Chao, *Phys. Rev. B* **61**, R2413(R) (2000).
- [14] A. A. Kiselev and K. W. Kim, *Phys. Rev. B* **61**, 13115 (2000).
- [15] S. Kettmann, *Phys. Rev. Lett.* **98**, 176808 (2007).
- [16] T. Schäpers, V. A. Guzenko, M. G. Pala, U. Zülicke, M. Governale, J. Knobbe, and H. Hardtdegen, *Phys. Rev. B* **74**, 081301(R) (2006).
- [17] Y. Kunihashi, M. Kohda, and J. Nitta, *Phys. Rev. Lett.* **102**, 226601 (2009).
- [18] J. Wunderlich, B.-G. Park, A. C. Irvine, L. P. Zarbo, E. Rozkotov, P. Nemeč, V. Novk, J. Sinova, and T. Jungwirth, *Science* **330**, 1801 (2010).
- [19] A. W. Holleitner, V. Sih, R. C. Myers, A. C. Gossard, and D. D. Awschalom, *Phys. Rev. Lett.* **97**, 036805 (2006).
- [20] C. P. Weber, N. Gedik, J. E. Moore, J. Orenstein, J. Stephens, and D. D. Awschalom, *Nature (London)* **437**, 1330 (2005).
- [21] L. Yang, J. D. Koralek, J. Orenstein, D. R. Tibbetts, J. L. Reno, and M. P. Lilly, *Nat. Phys.* **8**, 153 (2012).
- [22] M. P. Walser, U. Siegenthaler, V. Lechner, D. Schuh, S. D. Ganichev, W. Wegscheider, and G. Salis, *Phys. Rev. B* **86**, 195309 (2012).
- [23] A. V. Poshakinskiy and S. A. Tarasenko, *Phys. Rev. B* **92**, 045308 (2015).
- [24] G. Salis, M. P. Walser, P. Altmann, C. Reichl, and W. Wegscheider, *Phys. Rev. B* **89**, 045304 (2014).
- [25] M. M. Glazov and E. Y. Sherman, *Phys. Rev. Lett.* **107**, 156602 (2011).
- [26] P. Altmann, M. P. Walser, C. Reichl, W. Wegscheider, and G. Salis, *Phys. Rev. B* **90**, 201306 (2014).
- [27] P. Wenk and S. Kettmann, *Phys. Rev. B* **83**, 115301 (2011).
- [28] R. M. Lutchyn, J. D. Sau, and S. Das Sarma, *Phys. Rev. Lett.* **105**, 077001 (2010).
- [29] Y. Oreg, G. Refael, and F. von Oppen, *Phys. Rev. Lett.* **105**, 177002 (2010).
- [30] J. Alicea, *Phys. Rev. B* **81**, 125318 (2010).
- [31] V. Mourik, K. Zuo, S. M. Frolov, S. R. Plissard, E. P. A. M. Bakkers, and L. P. Kouwenhoven, *Science* **336**, 1003 (2012).
- [32] Y. Kunihashi, M. Kohda, H. Sanada, H. Gotoh, T. Sogawa, and J. Nitta, *Appl. Phys. Lett.* **100**, 113502 (2012).
- [33] P. Chuang, S.-C. Ho, L. W. Smith, F. Sfigakis, M. Pepper, C.-H. Chen, J.-C. Fan, J. P. Griffiths, I. Farrer, H. E. Beere, G. A. C. Jones, D. A. Ritchie, and T.-M. Chen, *Nat. Nanotechnol.* **10**, 35 (2014).